Assessment of the Pathophysiology of Injured Tissue With an *In Vivo* Electrical Injury Model

Thu T. A. Nguyen, Jeffrey W. Shupp, Lauren T. Moffatt, Marion H. Jordan, Ellen J. Leto, and Jessica C. Ramella-Roman

***Abstract*—Tissue destruction from electrical injury is devastating and hard to treat. Unfortunately, the pathophysiology of electrical trauma is still not well understood. We have developed a suite of tools aimed at investigating damage due to high voltage shock on the skin using a rat model. Electrical injuries were created with a custom made high-tension shock system and a spectroscopic system, based on spatial frequency domain imaging, was used to determine optical properties of electrically injured tissues. The extrapolated values of absorption and scattering coefficients at six different wavelengths were then utilized to monitor parameters of interest such as tissue oxygen saturation, methemoglobin volume fraction, and hemoglobin volume fraction at four time intervals post injury. An FLIR thermal camera was used to record skin temperature during the electrical shock. Finally, a laser Doppler imaging apparatus was used to assess tissue perfusion. In this paper, the results of experiments conducted on a rat model and discussions on the systemic changes in tissue optical properties before and after electrical shock are presented. A reduction in tissue oxygen saturation postinjury is observed as well as an increase in methemoglobin. Tissue perfusion increases immediately after the delivery of the electrical shock.**

***Index Terms*—Electrical burns, laser Doppler imaging (LDI), methemoglobin, spatial frequency domain imaging (SFDI), thermal response.**

I. Introduction

ELECTRICAL accidents are a significant cause of occupational injury and death, despite regulations and safety measures. From 1992 to 2002, 3378 workers died from occupational electrical injuries. This type of injury is often associated with systemic effects on patient's body affecting multiple organs. Generally, the heart, the skin, and nervous tissues are the most commonly impacted organs causing a chain of events that can lead to patient suffering and eventually death.

Manuscript received September 1, 2011; revised November 14, 2011; accepted December 2, 2011. Date of publication December 13, 2011; date of current version July 10, 2012. This work was supported by the PEPCO Holdings, Inc., and the DC Firefighters Burn Foundation.

T. T. A. Nguyen is with the Department of Electrical Engineering, The Catholic University of America, Washington, DC 20064 USA (e-mail: 19nguyen@cardinalmail.cua.edu).

J. W. Shupp, L. T. Moffatt, and E. J. Leto are with Burn Center, Department of Surgery, Washington Hospital Center, MedStar Health Research Institute, Washington, DC 20010 USA (e-mail: jeffrey.w.shupp@medstar.net; lauren.t.moffatt@medstar.net; Ellen.J.Leto@medstar.net).

M. H. Jordan is with Burn Center, Department of Surgery, Washington Hospital Center, MedStar Health Research Institute, Washington, DC 20010 USA, and also with Georgetown University, Washington, DC 20057 USA (e-mail: marion.h.jordan@medstar.net).

J. C. Ramella-Roman is with the Department of Biomedical Engineering, The Catholic University of America, Washington, DC 20064 USA (e-mail: ramella@cua.edu).

Digital Object Identifier 10.1109/JSTQE.2011.2179525

Lee and Dougherty [1] showed that the extent of tissue damage depends on current's pathway, strength, and duration. Basically, the direct mechanisms for tissue injury are strong electric field effects on protein and cellular structures, while the indirect mechanism of injury has been identified as Joule heating. Lee *et al*. also helped to demonstrate both thermal and nonthermal tissue damage under high-voltage electrical shock [2]–[8]. A problem, particular to electrical injury, is that damage is often seen at locations distant from the site of injury, a fact that once recognized may help improve survival.

To date, several animal models have been used to investigate tissue damage from electrical exposure. A rat model has been developed by Kalkan *et al*. [9] to study the dynamics of thermal response for body components in electric injury mechanisms. Subsequent change in muscle perfusion and pathophysiology was considered. A 330-mA current was applied to each rat for 10 s at 440 V. The results showed a sudden increase of temperature in muscle (from $35.3 \pm 1.2\,^{\circ}\mathrm{C}$ to $75.2 \pm 7.6\,^{\circ}\mathrm{C}$) that was greater than the increase in bone and core. Additionally, muscle perfusion reached the minimum level at 72 h after shock and the right hind limb exhibited more damage than the left fore limb. In the report of Fan *et al*. [10] on electrical injuries to peripheral nerves, high voltages of 3600, 1000, and 500 V were respectively applied to the right sciatic nerve of rats for 10 ms. It was shown that by the fourth week after injury, digit ulcers appeared in the rats receiving 3600- and 1000-V shocks. The neural conduction velocity disappeared immediately after injuries, but recovered to 65% with 500-V rats, 7% with 1000-V rats, and not at all with 3600-V rats. Finally, it was found that blood vessel embolisms occurred. Block *et al*. [11] applied pulsed electric fields of approximately 150 V/cm in hind limbs of rats and showed that the electroporation effects on muscle necrosis were a nonthermally mediated factor. In the research on electric current arterial injury of Buchanen *et al*. [12], an electrical circuit was used to deliver 50–500 V alternating current to rats. Chen *et al*. [13] established a standardized 10-kV, 5-s electric burn rabbit model in order to observe the resulting cellular necrosis. To investigate the mechanism of electrical injuries, Li *et al*. [14] used a rabbit model in which different high voltage shock durations and sizes of electrode areas were applied, and resulting variable damage was examined. In our laboratory, we built and tested a precise and controllable high-voltage direct current shock system, which was originally tested on porcine skin samples and, subsequently, in rats, and described in detail in previous publications [15], [16].

Presently, it is still a clinical challenge to determine the viability of soft tissue that is adjacent to entry and exit wounds. In

addition to visual assessment methods, a variety of diagnostic imaging modalities have been developed to aid in the evaluation soft tissue injury. Thermography can assess burn depth in correlation to temperature with an accuracy of up to 90%. However, this method has major limitations, particularly due to ambient heat loss and sensitive timing [17]. Radiotracer imaging is considered an appropriate noninvasive tool for quantifying the extent of electroporation injury [18]. Magnetic resonance imaging is a valuable tool for visualizing the extent of deep tissue damage in order to guide a surgical procedure. These functional images present the physiological behavior of an organ system [18], and have been used by several groups [19]–[22]. Ultrasound can be used to distinguish between necrotic and viable tissue based on the acoustic impedance of the tissue. However, this tool requires contact with the patient and is, therefore, not desirable for this application [23], [24]. Jia-Ke *et al*. used microscopy to observe the pathological changes of soft tissue injury from a high-voltage electrical burn [25]. In another study, Sugata *et al*. [26] utilized a laser confocal scanning microscope for their research on subepidermal wound healing observation.

Laser Doppler imaging (LDI), used to measure blood perfusion, is a useful and accurate noninvasive tool for evaluating burn wounds as well as differentiating viable and nonviable injuries [27]–[30]. However, LDI measurements may be affected by the curvatures of tissue, wound infection, topical substances, wound humidity, movement of the object, distance from wound, and angle of recording [17], [29]. Optical coherence tomography (OCT) can provide high-resolution cross-sectional images of tissue microstructure [31] and an OCT scanner can be used to generate volumetric images of the tissue. However, in OCT, the penetration depth is very shallow and is confined to the upper layers of the skin. Indocyanine green video angiography has been considered an accurate mean for dermal viability determination with high sensitivity [17] but requires dye injection [32] and is, hence, considered an invasive method. Photoacoustic microscopy (PAM) has been used, recently, by some burn injury monitoring researchers [33]–[37]. This technique is directly related to the absorption coefficient in the tissue, which is used to determine physiological properties such as oxygen saturation and hemoglobin concentration [38]. PAM shows the potential for high-resolution imaging at high depth but similarly to ultrasound has the drawback of acoustic attenuation and ultrasound transducer contact.

Some other promising optical imaging techniques have been, recently, introduced for burn depth assessment such as near infrared spectroscopy (NIRS) [27], multispectral imaging [27], [39], [40], and spatial frequency domain imaging (SFDI) [32], [41]. NIRS has the advantage of deep penetration by utilizing near infrared light, while multispectral imaging can provide abundant optical information about burn wounds along several wavelengths. Based on the attenuation of light in tissue, the concentration of the chromophores can be determined [27]. However, the main limitation of these techniques is that absorption coefficient and scattering coefficient cannot be distinguished and calculated directly from the collected images, so ad hoc models are often used. Moreover, NIRS may require physical probe contact with the wound [32]. SFDI is a new noninvasive imaging technique which can provide optical properties of injured tissue at different depths of penetration. Parameters like oxyhemoglobin, deoxyhemoglobin, and water can be measured, and 3-D maps of both perfusion and metabolic activity within a tissue can be constructed [32].

SFDI has been previously described for use in imaging of chronic wounds and subsurface heterogeneities. In 2009, this technique was successfully applied by Cuccia *et al*. [41] for quantification and mapping of tissue optical properties. In our publication, SFDI was used for oxygen saturation determination of blood vessels in the human retina [42]. Studies on pedicle cutaneous flaps of rats before and after vascular occlusion showed the capability of SFDI in quantification and detection of physiologic changes [32], [43], [44].

In this study, we propose the utility of SFDI for assessing the pathophysiologic changes in wounds adjacent to electrical contact burns. The changes of oxygen saturation, hemoglobin volume fraction, and methemoglobin at the sites near the wound were observed at different time points before and after high-voltage electrical shock. Additionally, LDI images were simultaneously acquired to collate with SFDI data for further consideration and comparison. A thermal camera was also used to monitor the skin temperature during electrical shocks.

II. Material and Methods

An experimental model was built to produce and examine electrical injuries on anesthetized rats. This apparatus included an electrical burn delivery system (EBDS), described in [16], able to deliver 1000 V of dc for different periods of time (from 2 to 20 s), a thermal camera (FLIR, Breda, The Netherlands) to record changes in skin temperature during shock, a SFDI system at visible range to capture images for skin optical properties, and a LDI system to show blood flow. The last two tools were utilized to image wounds at five time points: before, immediately after, and 1, 2, and 3 h after shock. A simple layout of the experimental setup is illustrated in Fig. 1. Details of each component in our system are introduced in the following.

A. SFDI System

Our SFDI system included a white LED light source (Enfis, Swansea, U.K.) aligned to a liquid crystal display screen (LCD Kit, BBS, Bad Wiesse, Germany, 350:1 maximum contrast, 1024 pixel $\times$ 768 pixel resolution) and a projection lens ($f = 45$ mm) to focus a spatially varying patterns onto the samples. These components were fixed into a light tight enclosure. A 2-D sinusoidal pattern was created in MATLAB (16-bit resolution) and sent to the LCD. A scientific cooled CCD camera (Photometrics Cascade 1 K, Tucson, AZ, resolution 1002 pixel $\times$ 1004 pixel, pixel size: 8 μm $\times$ 8 μm) and an imaging lens ($f = 25$ mm) were used to image the samples. The camera was capable of 9 frames/s acquisition at 16-bit resolution of an area 17 mm $\times$ 17.5 mm. A liquid crystal tunable filter (CRI, Woburn, MA) in front of the camera was computer controlled to allow sequential selection of different wavelengths from 400 to 700 nm with 7-nm bandwidth.

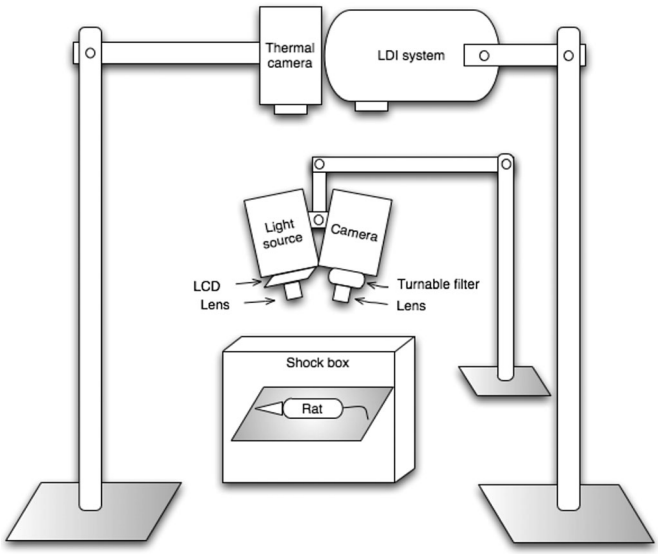

Fig. 1. Layout of the experimental setup.

In order to avoid specular reflection from the sample, cross polarizers and a slight angle between the projection part and the imager were also used. The projection angle was set up at 5° while the imaging angle was approximately 12°. The small angle chosen for incident light is to diminish the attenuation and phase shift of sinusoidal fringe patterns in the turbid media [45]. The working distance of the system is 8 ± 0.5 cm.

The whole system was integrated onto a movable arm for flexible positioning and was controlled through a user interface written in MATLAB.

One of the drawbacks of an LCD projector is the screen-door effect, which creates a microgrid at high spatial frequency on the sample. This effect was diminished by applying a second-order low-pass filter of 5-Hz cutoff frequency and 200-Hz sampling frequency during data analysis. Tests on optical phantoms described later also show that this not an important problem for quantitative assessment of optical properties.

Skin is a diffusive media, where the scattering coefficient dominates the absorption coefficient; an approach based on the diffusion equation [41] can then be utilized.

In order to obtain optical properties of a sample, SFDI utilizes a sinusoidal pattern illumination. Three different patterns were used at three phases 0, $2\pi/3$, and $4\pi/3$ rad at one fixed spatial frequency f_x. A known optically diffusive phantom was also used as a reference and to normalize the collected images. Three images at three phases of the sample and those of the reference were acquired by our system for postanalysis. At each pixel of the captured images, the spatially modulated (ac) and planar (dc) reflectance terms were determined. These ac and dc components were used to extrapolate diffuse reflectance of the sample based on known diffuse reflectance of the reference. Absorption coefficient μ_a and reduced scattering coefficient μ_s' at that pixel are achieved by using a minimization algorithm [46] on the diffusion equation [41].

According to Cheong data on optical properties of rat skin [47], the minimum value of transport coefficient $\mu_{\rm tr}$ ($\mu_{\rm tr} = \mu_a + \mu_s'$) over the range of wavelengths between 355 and 1064 nm is 0.93 $\rm mm^{-1}$. Therefore, the spatial frequency of sinusoidal patterns was chosen at 0.33 $\rm mm^{-1}$ to satisfy the condition of frequency and transport coefficient $f_x \ll \mu_{\rm tr}$ [41]. Such a spatial frequency would be sufficiently small to meet the condition even with large variation of $\mu_{\rm tr}$ of rat skin. Moreover, the spatial frequency is also considered to establish sampling depth, as will be explained later in this paper.

In this study, we utilized visible light at six wavelengths 470, 507, 522, 549, 620, and 650 nm to easily observe the distinction inherent in oxygenated (oxy) and deoxygenated (deoxy) hemoglobin. The effective penetration depth $\delta_{\rm eff}'$ is expressed as a function of μ_a, μ_s', and f_x

$$\frac{1}{\delta_{\rm eff}'} \equiv \mu_{\rm eff}' = \left(\mu_{\rm eff}^2 + k^2\right)^{1/2} \tag{1}$$

where $k = 2\pi f_x$ is the wavenumber, and $\mu_{\rm eff} = (3\mu_a\mu_{\rm tr})^{1/2}$. μ_a and μ_s' of rat skin decrease with respect to the wavelength of illumination in the range of 470–650 nm. Therefore, the maximum effective penetration depth (475.3 μm) is obtained at the minimum μ_a and μ_s', which are 0.02 and 2.1 $\rm mm^{-1}$ at 650 nm, respectively, and the minimum effective penetration depth (379.2 μm) is obtained at the maximum μ_a and μ_s', which are approximately 0.13 and 6.7 $\rm mm^{-1}$ at 470 nm [47]. The thickness of the rat epidermis alone was reported [48] in the ranges of 13.8 ± 2.2 to 22.7 ± 3.4 μm (age of 5–180 days), while the thickness of epidermis and dermis combined ranged from 276 ± 31 to 832 ± 73 μm. Hence, the maximum and the minimum effective penetration depths of our system are both within the upper portion of the dermal layer of the rat skin. We also want to point out that several authors [49], [50] have noted that in a layered structure such as the skin, crosstalk may occur when extrapolating optical properties particularly when observing highly pigmented human skin. In this study, we used shaved rats, whose skin contained very little melanin and appeared light pink; furthermore, rat epidermis is $\sim$20 μm in thickness; hence, we believe this effect to be minimal in our studies.

1) Optical Property Measurements in Phantoms: To test the ability of our SFDI system to reconstruct optical properties, we conducted measurements on homogeneous polyurethane phantoms [51] (of known absorption coefficients in the range of 0.076–0.5 $\rm mm^{-1}$ and scattering coefficients in the range of 2.12–8 $\rm mm^{-1}$). The experimentally measured μ_a and μ_s' of six phantoms at two wavelengths 522 and 630 nm are showed in Fig. 2 and are compared to measurements of the same phantoms done with integrating sphere and inverse adding-doubling (IAD) [51]. IAD is a technique used to calculate the optical properties of a slab of material from measured transmission and reflection.

A second set of phantoms containing blood and microspheres was also constructed and measured with our system. These phantoms were built to have optical properties similar to the rat skin by using stabilized human ferrous hemoglobin (Sigma, St. Louis, MO) for absorption and microsphere solution (1.0 μm, Polybead Polystyrene Microspheres, Polysciences, Inc., Warrington, PA) as a scatter. Different amount of stabilized human ferrous hemoglobin were mixed with deionized water to create different concentrations of hemoglobin solutions. Sodium

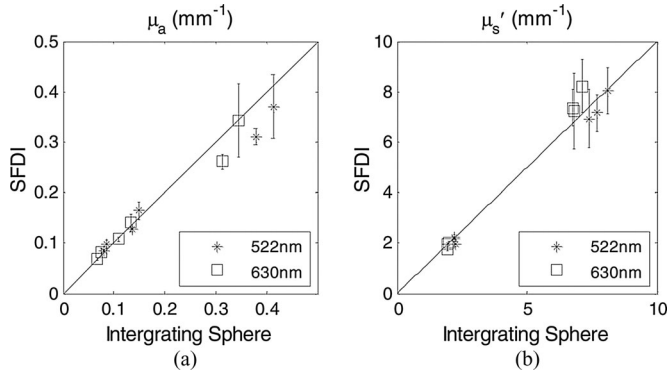

Fig. 2. Calibration results of (a) absorption coefficients and reduced (b) scattering coefficients on six phantoms.

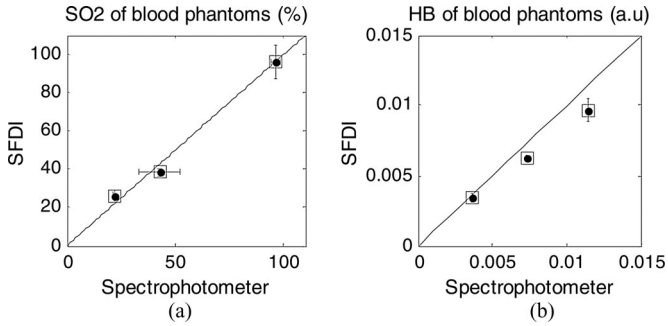

Fig. 3. (a) SO_2 of blood phantoms measured from spectrophotometer and SFDI system. (b) HB volume fraction of blood phantoms measured from spectrophotometer and SFDI system.

hydrosulfite (Sigma) was then gradually added to the liquid mixture to reduce oxygen content. The same concentration of microspheres was added to all the samples.

The phantoms were divided into two groups; the first group included three phantoms that had an oxygen saturation level of nearly 100% (no sodium hydrosulfite added) and three different hemoglobin concentrations (1, 2, and 3 mg/ml). The second group consisted of three phantoms that had the same hemoglobin concentration but different oxygen saturation levels, approximately 100%, 40%, and 20%. No sodium hydrosulfite was added to have nearly 100% SO_2.In order to reach 40% and 20% SO_2, amounts of sodium hydrosulfite added to blood phantoms were 60 and 120 mg, respectively, for each 1-ml solution.

Values of oxygen saturation (SO_2) and hemoglobin (HB) volume fraction in each hemoglobin mixture were obtained using a spectrophotometer (Pharmacia Ultrospec 3000, Pharmacia Biotech, Uppsala, Sweden) and the SFDI system. Data from the spectrophotometer were later used to verify SFDI data. Before adding the microspheres, each hemoglobin solution was first placed into a 2-mm thickness glass cuvette, and optical density of the solution was measured. The absorption coefficient of the solutions was calculated at six wavelengths: 470, 507, 522, 549, 620, and 650 nm. In order to add microsphere solution into each sample without influencing the hemoglobin concentration of that sample, six identical samples were built where the deionized water amount was reduced in each sample and replaced with the microsphere solution. The final concentration of 1-μm microsphere is 0.016 spheres/μm^3 solution. Our SFDI system was then utilized to image these latter samples and optical properties were determined at all wavelengths.

The achieved absorption coefficients from the spectrophotometer and the SFDI system were computed for SO_2 and HB volume fraction by least square fitting with tabulated values of oxy- and deoxy-hemoglobin absorption coefficients $\eta_{a\mathrm{HB}}$ and $\mu_{a\mathrm{HBO}_2}$ [52] using the Nelder–Mead simplex minimization algorithm [46] and

$$\mu_a = B \times [(1-S) \times \mu_{a\mathrm{HB}} + S \times \mu_{a\mathrm{HBO}_2}] + C \quad (2)$$

where B represents HB volume fraction, S represents SO_2, and C is a fixed offset that represents skin background absorption.

For each sample, the spectrophotometer and SFDI measurements were conducted three times and mean values were extracted. Fig. 3 shows the results of these tests. Variable levels of HB volume fraction in group 1 and oxygen saturation in group 2 are observed in Fig. 3(a) and (b). Spectrophotometer and SFDI system provided similar results, although there were still some disparities, especially at high hemoglobin concentration with a percentage error up to 16%. The microsphere with sodium hydrosulfite and blood solutions showed visible aggregation of particles when unstirred over long periods of time, although the solution was thoroughly mixed before imaging the impact of aggregation is hard to control; we believe it may have contributed to the discrepancy in the results but other errors such at titration and evaporation may also contribute to the difference in results.

B. Methemoglobin

Methemoglobin is formed due to the oxidation of the iron of the hemoglobin to its ferric state. Methemoglobin contains ferric iron residues (Fe^{3+}) instead of the normal ferrous iron (Fe^{2+}) which is found in deoxy- and oxy-hemoglobin. Methemoglobin constitutes only 1% of hemoglobin in a healthy individual and an elevated level of methemoglobin may cause symptoms such as impaired respiration, cyanosis, inflammation, atherosclerotic disease, and even death [27], [53], [54]. Some reports have shown the presence of methemoglobin in burn wounds. In an animal study on burn wound assessment using NIRS [27], the presence of methemoglobin was demonstrated as well as the relationship of methemoglobin with burn depth. However, many challenging questions surrounding the presence of methemoglobin remain. In this paper, we apply a least squares fitting method to verify the existence of methemoglobin in electrical burn injuries and assess its relative changes for 3 h after high-voltage electrical shock.

The model of skin absorption mentioned in (2) was modified by adding methemoglobin absorption (3), where W represents the methemoglobin volume fraction and $\mu_{a\mathrm{MetHB}}$ denotes the absorption coefficient of methemoglobin. Both tabulated values of $\mu_{a\mathrm{HB}}$, $\mu_{a\mathrm{HBO}_2}$, and $\mu_{a\mathrm{MetHB}}$ from an animal study [55] were used to fit the experimental results

$$\mu_a = B \times [(1-S) \times \mu_{a\mathrm{HB}} + S \times \mu_{a\mathrm{HBO}_2}] + W \times \mu_{a\mathrm{MetHB}} + C. \quad (3)$$

In this animal study, the absorption of melanin and water are neglected because of their insignificant contribution in comparison with the absorption of the other chromophores (oxy-, deoxy-hemoglobin, and methemoglobin).

C. Animal Experiments

An animal study was conducted under the approval of the MedStar Health Research Institute's animal care and use committee. A total of ten male Sprague-Dawley rats, all healthy and of approximately the same weight of 300 g and age of three months, were anesthetized and well-shaved and depilated at contralateral upper and lower extremities to avoid the effect of hair on the images. The animals were then positioned and fastened prone on a black felt board to reduce light interference from the background. The board was kept at the same position so that LDI as well as the SFDI system could measure the same area of skin during the experiment. Body temperature was observed by an infrared thermometer gun and kept at approximately 35 °C by a heating pad placed underneath the animal. The experiment was conducted in an animal procedure room and followed the standard operating procedures and laboratory protocol.

Using the previously described EBDS system [16], two stainless steel electrodes were fixed to the appropriate limbs, and a shock of 1000 V_{DC} was delivered between the left upper limb and the right hind limb of each animal. Ten rats were divided into four groups exposed to high voltage at various time durations; 2-s shocks for group I (2 rats), 4-s shocks for group II (3 rats), 8-s shocks for group III (3 rats), and 20-s shocks for group IV (2 rats).

III. Results and Discussion

All animals survived the electrical shock and the subsequent 3 h. The thighs adjacent to the wounds on right hind limbs were monitored by SFDI and LDI scanning system before, immediately after, and every hour up to 3 h after the injury.

A. Thermal Results

Changes in temperature of skin were measured using the thermal camera. These measurements were taken in the same areas of the skin that were subsequently imaged. The mean values of temperature (in Celsius) in the region of interest of each animal were determined and the average of mean values for all of the animals in each exposure group was calculated. Changes in temperature are presented as the differences from baseline (see Fig. 4). Standard deviation of the means for each group was also calculated. Results indicate that skin temperature increases with increasing shock duration and the highest elevation of temperature was achieved with a 20-s shock. Groups exposed to short durations (group I and II) showed a mean increasing temperature of 3.6 and 6.8 °C from their baselines, while the groups exposed to longer durations (group III and IV) had a mean increasing temperature of nearly 10 and 20 °C from their baselines. The threshold for cellular injury due to thermal shock was pointed out by Tropea and Lee [2] at about 42 °C. The average baseline temperature of the rats used in these test was 35 °C; hence, we expect group III and IV (8 and 20 s) to suffer the highest cell damage.

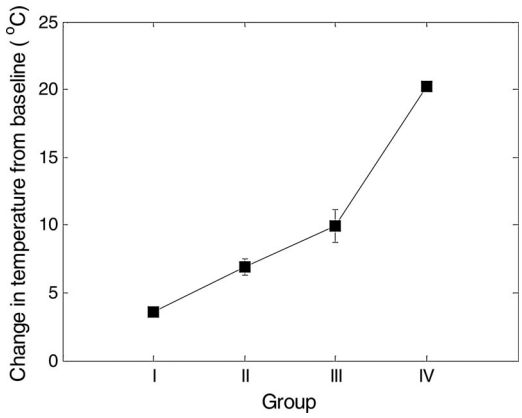

Fig. 4. Maximum changes in skin temperature during high voltage shock of all groups.

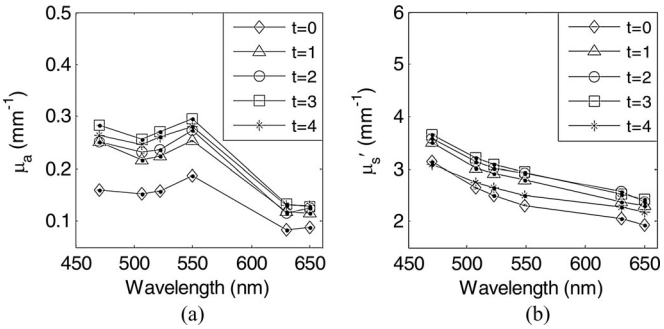

Fig. 5. (a) Absorption coefficients and reduced (b) scattering coefficients at six wavelengths of a wound at five periods of time: before ($t = 0$), right after ($t = 1$), and 1, 2, and 3 h ($t = 2$, 3, and 4) after shock.

B. SFDI Results

Acquired SFDI images were analyzed to monitor changes in optical properties at the observed skin areas. Fig. 5 illustrates mean values of absorption coefficients (a) and reduced scattering coefficients (b) of an animal wound at various time points: before ($t = 0$), immediately following ($t = 1$), and 1, 2, and 3 h ($t = 2$, 3, and 4) after a 1000 V_{DC} shock applied for 20 s. Standard deviations of the mean are also included in the graphs but are insignificant. The results are comparable to rat skin optical properties reported by Cheong *et al.* [47] which are 0.02–0.13 mm^{-1} for μ_a and 2.1–6.7 mm^{-1} for μ_s' in the range of our considered wavelengths. Increases in reduced scattering coefficients were observed in 70% of all animals immediately following shocks, whereas absorption coefficients for all animals increased remarkably (data not shown).

A hematoma appeared at the sites adjacent to injuries indicating a build up of blood in the skin. We believe bilirubin and methemoglobin may also be present. The bilirubin concentration is believed to be low in bruises containing methemoglobin [56]; hence, (3) was utilized to extrapolate oxygen saturation (SO_2), hemoglobin volume fraction (HB), and methemoglobin volume fraction (MetHB) from the achieved absorption coefficient

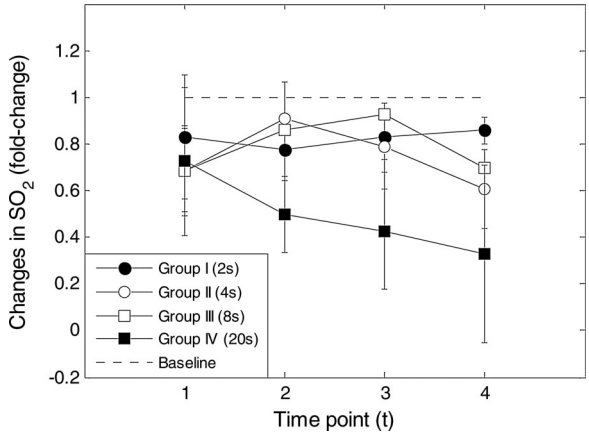

Fig. 6. Changes in SO_2, represented as fold change, of rats in all groups over time points: immediately after ($t = 1$), and 1, 2, and 3 h ($t = 2$, 3, and 4) after injury.

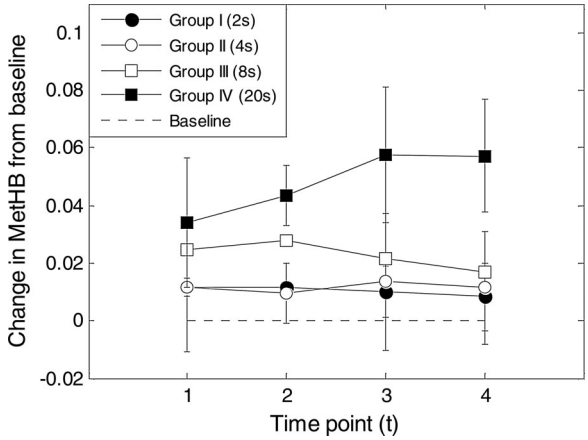

Fig. 7. Changes in MetHB of all groups over time points: immediately after ($t = 1$), and 1, 2, and 3 h ($t = 2$, 3, and 4) after injury.

results. Mean values and standard deviations of SO_2, HB, and MetHB of each group were calculated.

1) Oxygen Saturation Results: All animals exhibited a decline in SO_2 right after high voltage shock. SO_2 values at all time points for each animal are normalized by dividing by the initial SO_2 values at $t = 0$ (before injury) of that animal; this was done to observe the fold change from baseline.

Variations in SO_2 of all groups over the time points are shown in Fig. 6. Group IV suffering 20-s electrification is the only one showing a significant decrease in SO_2 while three other groups suffering 2-, 4-, and 8-s shocks, respectively, show similar fluctuations.

SO_2 levels of the rats receiving 2-s shocks decreased right after injury, but started recovering by the time point of 1 h after shock, whereas SO_2 levels of 20-s rats continued decreasing during the three subsequent hours.

2) Methemoglobin Volume Fraction Results: Results of MetHB of all groups indicate a small amount of methemoglobin present during the study period. Values vary from 0 to 0.05 at initial time point ($t = 0$). Because of existing zero values at $t = 0$, the variation of MetHB of each rat during three postinjury following hours was evaluated by subtracting postinjury MetHB values to initial values. The differences from baseline are observed. Fig. 7 shows the changes in MetHB of all groups over time points: immediately after ($t = 1$), and 1, 2, and 3 h ($t = 2$, 3, and 4) after injury. Results show increasing MetHB right after shocks ($t = 1$) for all groups. It is also apparent that MetHB increases with increasing shock duration. The mean values of MetHB for group I (2 s) and group II (4 s) indicate similar trends over time points before and after injury. MetHB values of animals receiving 8-s injuries showed a recovery of methemoglobin beginning at 1 h after injury ($t = 2$) but not much different from groups I and II, while MetHB levels in animals exposed for 20 s significantly increased after shock and for the subsequent three hours.

3) Hemoglobin Volume Fraction Results: HB values are expressed as fold change from a baseline ($t = 0$). Results do not show obvious trends of change of HB levels although the mean values of almost all the groups increased above the baseline (see Fig. 8).

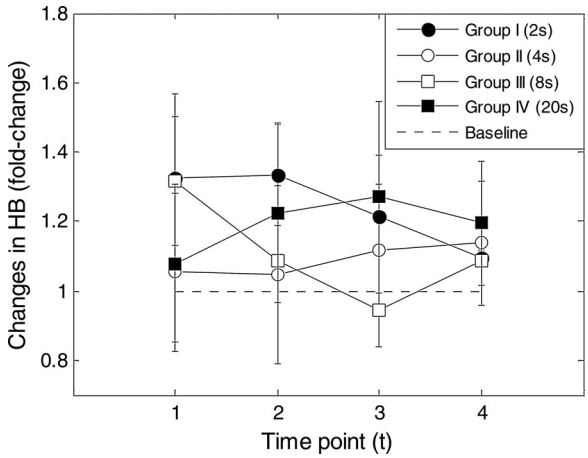

Fig. 8. Changes in HB, represented as fold change, of all groups over time points: immediately after ($t = 1$), and 1, 2, and 3 h ($t = 2$, 3, and 4) after injury.

We want to point out that the variability shown in these results is due in large part to the heterogeneity of our samples as results from different animals are averaged. In Fig. 8, volume fraction of hemoglobin increased immediately after injury and then decreased 1 h postinjury in group I, and 2 h postinjury in group IV. Similarly, no significant trend in HB was observed in groups II or IV.

C. LDI Results

LDI images were gathered in approximately the same area used as SFDI images. Regions of interest were selected in these areas. Means of perfusion units were calculated and changes in perfusion are presented as fold change. In rats exposed to short shock durations (2 and 4 s), perfusion appears to increase immediately postshock, followed by a gradual decrease over time. Groups exposed to longer shocks (8 and 20 s) show a decrease in perfusion, and remain fairly constant during the remainder of the time course (see Fig. 9). Similar trends to the one in Fig. 9 have been previously shown by Shupp *et al*. [16].

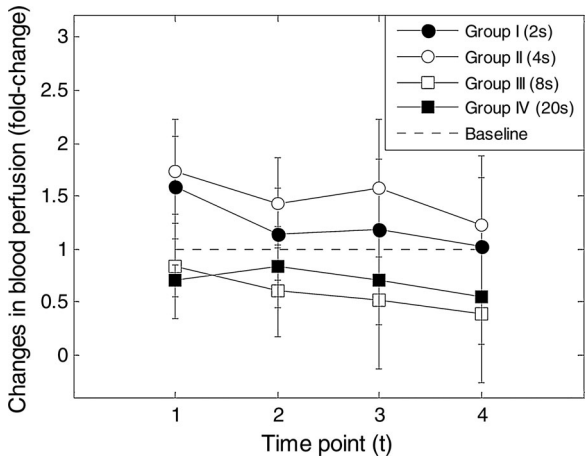

Fig. 9. Changes in perfusion, represented as fold changes, of all groups over time points: immediately after ($t = 1$), and 1, 2, and 3 h ($t = 2$, 3, and 4) after injury.

IV. Conclusion

A reliable EBDS was built and successfully delivered accurate high voltage shocks to fully anesthetized animals at preset voltages, currents, and exposure durations.

An SFDI system based on diffused reflectance was built and tested on polyurethane phantoms. Results show the feasibility of this imaging modality in monitoring the pathophysiology of tissue adjacent to electrical contact. The penetration depth was controlled to simultaneously monitor epidermal and dermal layers of rat skin.

Optical properties of the skin were obtained and agreed with previous published data. Absorption coefficients and reduced scattering coefficients changed dramatically after shock, indicating a significant impact on the physiology of the animal. This is in agreement with the assertion of Lee *et al*. [6] about recognizable changes of optical properties due to burn injuries. Both the absorption and scattering coefficients of the rat skin changed at all wavelengths. These changes correlate to perfusion analysis in areas adjacent to the wound sites and correlate with an inflammatory response. We speculate that substantial cell damage occurred in the groups of animals exposed to longer shock times (8 and 20 s), where an increase in temperature of up to 20 °C was noted. Interestingly, at low exposure time, changes in optical properties are still noted while the raise in temperature was modest; this could point to a different type of nonthermal damage. The results of oxygen saturation, methemoglobin volume fraction, and hemoglobin volume fraction are important surrogate metrics to tissue perfusion and oxygen delivery. In wounds, the balance of blood delivery, venous pressures, and cell viability is critical to tissue viability. Subtle changes in any of these metrics may provide early optical signatures that will help clinicians identify vulnerable tissue. If this is done early and noninvasively, treatments may be installed to save questionably viable areas adjacent to necrotic wounds.

A build up of methemoglobin and a reduction in oxygen saturation was noted in all animals subjected to shock. As documented in hematoma evolution and involution, methemoglobin is seen in the breakdown of hemoglobin molecules. In the setting of vulnerable cutaneous tissue, methemoglobin may represent the stasis of blood in the microvasculature beds. At times of increased local venous pressure, arterial pressure is not great enough to create net forward movement of blood. This static environment may cause extravasation of fluids, protein, and the break-down products of erythrocytes. Blood volume fraction seemed to increase over time, possibly due to the creation of a hematoma, or could also indicate the presence of a gradual vascular leakage.

Further analysis of these data along with physiological and molecular metrics will help correlate these noninvasive results with the phenotype of the lesions.

Acknowledgment

The authors would like to thank D. Smolley, P. Lemaillet, and A. Nalibi for their helps in the construction of the EBDS system and A. Basiri for his support and discussion.

References

[1] R. C. Lee and W. Dougherty, "Electrical injury: Mechanisms, manifestations, and therapy," *IEEE Trans. Dielectr. Electr. Insul.*, vol. 10, no. 5, pp. 810–819, Oct. 2003.

[2] B. I. Tropea and R. C. Lee, "Thermal injury kinetics in electrical trauma," *J. Biomech. Eng.*, vol. 114, no. 2, pp. 241–250, May 1992.

[3] R. C. Lee and R. D. Astumian, "The physicochemical basis for thermal and non-thermal burn injury," *Burns*, vol. 22, no. 7, pp. 509–519, 1996.

[4] R. C. Lee and M. S. Kolodney, "Electrical injury mechanisms: Dynamics of the thermal response," *Plastic Reconstr. Surg.*, vol. 80, no. 5, pp. 663–671, Nov. 1987.

[5] R. C. Lee and M. Kolodney, "Electrical injury mechanisms: Electrical breakdown of cell membranes," *Plastic Reconstr. Surg.*, vol. 80, no. 5, pp. 672–679, Nov. 1987.

[6] R. C. Lee, D. J. Jang, and J. Hannig, "Biophysical injury mechanisms in electrical shock trauma," *Annu. Rev. Biomed. Eng.*, vol. 2, pp. 477–509, 2000.

[7] R. C. Lee, "Injury by electrical forces: Pathophysiology, manifestations and therapy," *Current Probl. Surg.*, vol. 34, no. 9, pp. 677–764, Sep. 1997.

[8] R. C. Lee, "Cell injury by electric forces," *Ann. New York Acad. Sci.*, vol. 1066, pp. 85–91, Dec. 2006.

[9] T. Kalkan, M. Demir, A. S. Ahme, S. Yazar, S. Dervisoglu, H. B. Uner, and O. Cetinkale, "A dynamic study of the thermal components in electrical injury mechanism for better understanding and management of electric trauma: An animal model," *Burns*, vol. 30, no. 4, pp. 334–340, Jun. 2004.

[10] K. W. Fan, Z. X. Zhu, and Z. Y. Den, "An experimental model of an electrical injury to the peripheral nerve," *Burns*, vol. 31, no. 6, pp. 731–736, Sep. 2005.

[11] T. Block, J. Aarsvold, K. Matthews, R. Mintzer, P. River, M. Capelli-Schellpfeffer, R. Wollmann, S. Tripathi, C. Chen, and R. C. Lee, "Non-thermally mediated muscle injury and necrosis in electrical trauma," *J. Burn Care Rehabil.*, vol. 16, no. 6, pp. 581–588, Nov./Dec. 1995.

[12] D. Buchanen, E. Yucel, and M. Spira, "Electric current arterial injury: A laboratory model," *Plastic Reconstr. Surg.*, vol. 72, no. 2, pp. 199–207, Aug. 1983.

[13] G. Chen, Y. Wu, and X. Xu, "An experimental model of electric injury by high voltage," *Chin. J. Plastic Surg. Burns*, vol. 10, no. 3, pp. 209–211, May 1994.

[14] W. P. Li, M. S. Zhu, Z. X. Zhu, J. C. Guan, and X. G. Xu, "A series of models of non-thermal high voltage electrical injuries," *Burns*, vol. 32, no. 8, pp. 986–991, Dec. 2006.

[15] T. A. Nguyen, A. Basiri, and J. C. Ramella-Roman, "Imaging spectroscopy of thermal and electrical burns," in *Proc. SPIE*, 2010, vol. 7548, pp. 75480C-1–75480C-6.

[16] J. W. Shupp, L. T. Moffatt, T. Nguyen, J. C. Ramella-Roman, R. Hammamieh, S. A. Miller, E. J. Leto, D. Y. Jo, P. R. Randad, M. Jett, J. C. Jeng, and M. H. Jordan, "Examination of local and systemic in vivo responses to electrical injury using an electrical burn delivery system," *J. Burn Care Res.*, 2011, to be published.

[17] L. Devgan, S. Bhat, S. Aylward, and R. J. Spence, "Modalities for the assessment of burn wound depth," *J. Burns Wounds*, vol. 5, pp. 7–15, 2006.

[18] K. L. Matthews, J. N. Aarsvold, R. A. Mintzer, C. T. Chen, and R. C. Lee, "Tc-99m pyrophosphate imaging of poloxamer-treated electroporated skeletal muscle in an in vivo rat model," *Burns*, vol. 32, no. 6, pp. 755–764, Jul. 2006.
[19] M. Ohashi, J. Koizumi, Y. Hosoda, Y. Fujishiro, A. Tuyuki, and K. Kikuchi, "Correlation between magnetic resonance imaging and histopathology of an amputated forearm after electrical injury," *Burns*, vol. 24, no. 4, pp. 362–368, Jun. 1988.
[20] J. Weissenburger and P. F. Clement, "MRI correlates of electrical injury," *Arch. Clin. Neuropsychol*., vol. 13, no. 1, p. 134, 1998.
[21] T. Sahiner, T. Kurt, and L. S. Bir, "Reversible hyperintense T2 MRI lesions of basal ganglia after an electrical injury," *Burns*, vol. 28, no. 6, pp. 607–608, Sep. 2002.
[22] C. B. Freeman, M. Goyal, and P. R. Bourque, "MR imaging findings in delayed reversible myelopathy from lightning strike," *Amer. J. Neuroradiol*., vol. 25, no. 5, pp. 851–853, May 2004.
[23] T. S. Adams, J. V. Murphy, P. H. Gillespie, and A. H. Roberts, "The use of high frequency ultrasonography in the prediction of burn depth," *J. Burn Care Rehabil*., vol. 22, no. 3, pp. 261–262, May/Jun. 2001.
[24] J. H. Cantrell, Jr., "Can ultrasound assist an experienced surgeon in estimating burn depth?" *J. Trauma*, vol. 24, no. 9, pp. S64–S70, Sep. 1984.
[25] C. Jia-Ke, L. Li-Gen, G. Quan-Wen, S. Xiao-Peng, Z. Hai-Jun, S. Zhi-Yong, W. Zhi-Qiang, and Z. Cai, "Establishment of soft-tissue-injury model of high-voltage electrical burn and observation of its pathological changes," *Burns*, vol. 35, no. 8, pp. 1158–1164, May 2009.
[26] K. Sugata, T. Kitahara, and Y. Takema, "Changes of human skin in subepidermal wound healing process," *Skin Res. Technol*., vol. 14, no. 4, pp. 436–439, Nov. 2008.
[27] K. M. Cross, "Assessment of tissue viability in acute thermal injuries using near infrared point spectroscopy," Ph.D. dissertation, Inst. Med. Sci., Univ. Toronto, Toronto, Canada, 2010.
[28] S. A. Pape, C. A. Skouras, and P. O. Byrne, "An audit of the use of laser Doppler imaging (LDI) in the assessment of burns of intermediate depth," *Burns*, vol. 27, no. 3, pp. 233–239, May 2001.
[29] A. D. Jaskille, J. C. Ramella-Roman, J. W. Shupp, M. H. Jordan, and J. C. Jeng, "Critical review of burn depth assessment techniques—Part II. Review of laser Doppler technology," *J. Burn Care Res*., vol. 31, no. 1, pp. 151–157, Jan./Feb. 2010.
[30] Z. B. Niazi, T. J. Essex, R. Papini, D. Scott, N. R. McLean, and M. J. Black, "New laser Doppler scanner, a valuable adjunct in burn depth assessment," *Burns*, vol. 19, no. 6, pp. 485–489, Dec. 1993.
[31] B. H. Park, C. Saxer, S. M. Srinivas, J. S. Nelson, and J. F. deBoer, "In vivo burn depth determination by high-speed fiber-based polarization sensitive optical coherence tomography," *J. Biomed. Opt*., vol. 6, no. 4, pp. 474–479, 2001.
[32] M. Kaiser, A. Yafi, M. Cinat, and A. J. Durkin, "Noninvasive assessment of burn wound severity using optical technology: A review of current and future modalities," *Burns*, vol. 37, no. 3, pp. 377–386, May 2011.
[33] H. F. Zhang, K. Maslov, G. Stoica, and L. V. Wang, "Functional photoacoustic microscopy for high-resolution and noninvasive in vivo imaging," *Nature Biotechnol*., vol. 24, no. 7, pp. 848–851, 2006.
[34] M. Yamazaki, S. Sato, D. Saito, Y. Okada, A. Kurita, M. Kikuchi, and M. Obara, "Photoacoustic diagnosis of burns in rats: Two-dimensional photo-acoustic imaging of burned tissue," in *Proc. SPIE*, 2003, vol. 4960, pp. 7–13.
[35] L. V. Wang, *Photoacoustic Imaging and Spectroscopy*. Boca Raton, FL: CRC Press, 2009.
[36] J. T. Robert, H. H. Scott, and A. V. John, "Photoacoustic discrimination of viable and thermally coagulated blood using a two-wavelength method for burn injury monitoring," *Phys. Med. Biol*., vol. 52, no. 7, pp. 1815–1829, Apr. 2007.
[37] H. F. Zhang, K. Maslov, G. Stoica, and L. V. Wang, "Imaging acute thermal burns by photoacoustic microscopy," *J. Biomed. Opt*., vol. 11, no. 5, p. 054033, Sep./Oct. 2006.
[38] Photoacoustic Imaging Group, Univ. College London. [Online]. Available: http://www.medphys.ucl.ac.uk/research/mle/index.htm
[39] M. A. Afromowitz, J. B. Callis, D. M. Heimbach, L. A. DeSoto, and M. K. Norton, "Multispectral imaging of burn wounds: A new clinical instrument for evaluating burn depth," *IEEE Trans. Biomed. Eng*., vol. 35, no. 10, pp. 842–850, Oct. 1988.
[40] W. Eisenbeiss, J. Marotz, and J. P. Schrade, "Reflection-optical multispectral imaging method for objective determination of burn depth," *Burns*, vol. 25, no. 8, pp. 697–704, Dec. 1999.
[41] D. J. Cuccia, F. Bevilacqua, A. J. Durkin, F. R. Ayers, and B. J. Tromberg, "Quantitation and mapping of tissue optical properties using modulated imaging," *J. Biomed. Opt*., vol. 14, no. 2, pp. 024012-1–024012-13, Mar. 2009.
[42] A. Basiri, T. A. Nguyen, M. Ibrahim, Q. D. Nguyen, and J. C. Ramella-Roman, "Measuring the retina optical properties using a structured illumination imaging system," in *Proc. SPIE*, 2011, vol. 7885, p. 78851X.
[43] A. Yafi, T. S. Vetter, M. R. Pharaon, T. Scholz, S. Patel, and R. B. Saager, "Postoperative quantitative assessment of reconstructive tissue status in cutaneous flap model using spatial frequency domain imaging," *J. Plastic Reconstr. Surg*., vol. 127, no. 1, pp. 117–130, Jan. 2011.
[44] M. R. Pharaon, T. Scholz, S. Bogdanoff, D. Cuccia, A. J. Durkin, D. B. Hoyt, and G. R. Evans, "Early detection of complete vascular occlusion in a pedicle flap model using quantitative spectral imaging," *Plastic Reconstr. Surg*., vol. 126, no. 6, pp. 1924–1935, Dec. 2010.
[45] A. Bassi, D. J. Cuccia, A. J. Durkin, and B. J. Tromberg, "Spatial shift of spatially modulated light projected on turbid media," *J. Opt. Soc. Amer. A*, vol. 25, no. 11, pp. 2833–2839, 2008.
[46] J. A. Nelder and R. Mead, "A simplex method for function minimization," *The Comput. J*., vol. 7, no. 4, pp. 308–313, 1965.
[47] W. F. Cheong, S. A. Prahl, and A. J. Welch, "A review of the optical properties of biological tissues," *IEEE J. Quantum Electron*., vol. 26, no. 12, pp. 2166–2185, Dec. 1990.
[48] T. Ngawhirunpat, T. Hatanaka, K. Katayama, H. Yoshikawa, J. Kawakami, and I. Adachi, "Changes in electrophysiological properties of rat skin with age," *Biol. Pharm. Bull*., vol. 25, no. 9, pp. 1192–1196, Sep. 2002.
[49] R. B. Saager, A. Truong, A. J. Durkin, and D. J. Cuccia, "Method for depth-resolved quantitation of optical properties in layered media using spatially modulated quantitative spectroscopy," *J. Biomed. Opt*., vol. 16, pp. 077002-1–077002-8, 2011.
[50] J. Weber, D. Cuccia, A. Durkin, and B. Tromberg, "Noncontact imaging of absorption and scattering in layered tissue spatially modulated structured light," *J. Appl. Phys*., vol. 105, pp. 102028-1–102028-9, 2009.
[51] T. Moffitt, Y. C. Chen, and S. A. Prahl, "Preparation and characterization of polyurethane optical phantoms," *J. Biomed. Opt*., vol. 11, no. 4, pp. 041103-1–041103-10, Aug. 2006.
[52] S. L. Jacques. Spectroscopic determination of tissue optical properties using optical fiber spectrometer. [Online]. Available: http://omlc.ogi.edu/news/apr08/skinspectra/index.html
[53] R. O. Wright, W. J. Lewander, and A. D. Woolf, "Methemoglobinemia: Etiology, pharmacology, and clinical management," *Ann. Emergency Med*., vol. 34, no. 5, pp. 646–656, Nov. 1999.
[54] J. Umbreit, "Methemoglobin—it's not just blue: A concise review," *Amer. J. Hematol*., vol. 82, no. 2, pp. 134–144, Feb. 2006.
[55] S. A. Prahl, Oregon Medical Laser Center, private communication, Sep. 2010.
[56] L. L. Randeberg, A. Winnem, S. Blindheim, O. A. Haugen, and L. O. Svaasand, "Optical classification of bruises," in *Proc. SPIE*, 2004, vol. 5312, pp. 54–64.

Thu T. A. Nguyen received the B.E.E. degree in electrical engineering from the University of Danang, Danang, Vietnam, in 2006. She is currently working toward the Ph.D. degree in electrical engineering at the Catholic University of America, Washington, DC.

She collaborates with the Burn Center, Department of Surgery, Washington Hospital Center, MedStar Health Research Institute, Washington. Her current research interests include imaging and modeling of thermal and electrical burn injuries.

Jeffrey W. Shupp received the Medical degree from the Medical College of Virginia, Richmond.

He completed a training fellowship in molecular pathology at the Walter Reed Army Institute of Research. After graduation from the Medical School of Virginia, he began surgical residency training at Washington Hospital Center and completed a fellowship in burn surgery. Since 2008, he has been the Director of the Firefighters' Burn and Surgical Research Laboratory and an active Clinical Investigator with the MedStar Health Research Institute, Washington, DC. He is also an Adjunct Assistant Professor of biomedical engineering at the Catholic University of America. His research interests include wound healing, host-responses to traumatic injury, systems biology, scar pathophysiology, and surgical infections.

Lauren T. Moffatt received the B.S. degree in environmental science and policy from the University of Maryland, College Park, and the Ph.D. degree from the University of Massachusetts Amherst, Amherst, in 2003 and 2008, respectively.

She is currently with the Burn Research Laboratory, MedStar Health Research Institute, Washington, DC, where she is a laboratory Research Scientist. Her research interests include biomarkers of exposure and injury and the use of omics technologies.

Marion H. Jordan received the B.A. degree in chemistry from the West Georgia College, Carrollton, and the M.D. degree from the Medical College of Georgia, Augusta, in 1965 and 1969, respectively.

He has been the Director of the Burn Center, Washington Hospital Center, Washington, DC, for more than 30 years. He is also a Professor of surgery at Georgetown University, Washington, and Adjunct Associate Professor at the Uniformed Services University of the Health Sciences, Bethesda, MD. From 1979 to 2004, he was an Associate Clinical Professor of surgery at George Washington University.

Ellen J. Leto received the B.A. degree in public relations and international studies from Pennsylvania State University, University Park, in 2009.

She did a Postbaccalaureate Premedical Certificate Program at Georgetown University, Washington, DC. She is currently with the Burn Center, Department of Surgery, Washington Hospital Center, MedStar Health Research Institute, Washington. She has been involved in research in burns and wound healing since early 2010 and has an interest in laboratory animal care and noninvasive wound assessment technology.

Jessica C. Ramella-Roman received the Laurea degree in electrical engineering from the University of Pavia, Pavia, Italy, in 1993, and the Master and Ph.D. degrees in electrical engineering from Oregon Health and Science University, Portland, in 2004.

She was a Postdoctoral Fellow at the Applied Physics Laboratory, Johns Hopkins University. In 2006, she joined the Catholic University of America, Washington, DC, where she is currently an Associate Professor in the Department of Biomedical Engineering. She is also an Adjunct Assistant Professor at the Johns Hopkins School of Medicine, Baltimore, MD. Her current research interests include polarized light imaging, modeling of light transport into scattering and rough media, and the use of spectroscopic methodologies for monitoring skin and retinal disease.